Molecular Dynamics Simulation of Pre-existing Vacancy on Microwave Interaction with 3C-SiC: Role of Si-vacancy and Performance Comparison with C-vacancy

T L Dora[1], Akarsh Verma[2, 4], Tribeni Roy[1, 3], Saurav Goel[3, 4], Hamed Yazdani Nezhad[5], Stefania Castelletto[6], Radha Raman Mishra[1*]

[1]Department of Mechanical Engineering, Birla Institute of Technology and Science Pilani, Pilani-333031, India.

[2]Department of Mechanical Science and Bioengineering, Graduate School of Engineering Science, Osaka University, Osaka 560-8531, Japan

[3]School of Engineering, London South Bank University, London, SE10AA, United Kingdom.

[4]University of Petroleum and Energy Studies, Dehradun, 248007, India.

[5]School of Mechanical Engineering, Faculty of Engineering and Physical Sciences, University of Leeds, Leeds, LS2 9J, United Kingdom.

[6]School of Engineering, RMIT University, Melbourne, VIC 3001, Australia.

[*] Corresponding authors: rraman.mishra@pilani.bits-pilani.ac.in

Abstract

Microwave heating of 3C-SiC significantly influences its thermos-physical and electromechanical properties. However, the role of pre-existing vacancies in microwave heating of 3C-SiC systems remains inadequately understood. In this work, a molecular dynamics approach has been used to study the effect of pre-existing Si-vacancy on microwave interaction with the 3C-SiC system at Si-vacancy concentrations (0.5%, 1.0%, 1.5%, and 2.0%). The Si vacancy-induced 3C-SiC system was exposed to microwaves at different electric field strengths of 0.1 and 0.5 V/Å and frequencies of 100 GHz, 150 GHz, 200 GHz, 250 GHz, and 300 GHz. It was observed that microwave heating accelerates with increases in Si vacancy concentration, electric field strength, and frequency. Mean square displacement, diffusion coefficient, and radial distribution function were analysed to assess the physical properties and phase change in the 3C-SiC system during microwave exposure. The 2% Si vacancy provides the highest self-diffusion coefficient at 0.5 V/Å and 300 GHz than concentrations 0.5% (thrice), 1.0% (twice), and 1.5% (1.33 times). The phase and structural (40% to 50%) changes were observed during microwave exposure of the 3C-SiC system having 1.5% and 2.0% Si-vacancies for 4.985 ns and 4.49 ns,

respectively, at 0.5 V/Å and 300 GHz. Comparative performance evaluation of Si vacancy with C vacancy revealed that microwave heating of C-vacancies (1.5%, and 2% C) induced 3C-SiC system occurs at higher rates 95.5% and 142.2% respectively at 0.5 V/Å and 300 GHz as compared to same Si vacancies. Additionally, beyond 1000K, microwave heating in a C vacancy-based 3C-SiC system is driven by structural changes induced by vacancies as compared to the thermal conductivity of the system.

Keywords: microwave energy, atomistic modelling, silicon carbide, vacancy, thermal property

Graphical abstract

1 Introduction

Microwave processing of materials has attracted the research community globally due to the unique ability of microwaves to penetrate into the core of the material directly, resulting in rapid and volumetric heating of the target materials [1–4]. Moreover, microwave energy-based processing of the material is well-known for its low energy consumption, more uniform heating and short processing time as compared to conventional heating methods [5,6]. However, the efficient use of microwave energy for material processing is not as straightforward as it might seem, owing to the unpredictable interaction behaviour of microwaves when exposed to different

materials and their constituents [6,7]. Metallic materials, polymers, and their composites tend to behave as reflectors, transparent, or partial absorbers of microwave irradiation. On the contrary, ceramics such as SiC, and ZnO are excellent absorbers of microwave energy [8,9] due to their high thermal stability, excellent mechanical strength, chemical resistivity and wide band gap [10–13]. Subsequently, SiC is often utilised as a susceptor material in processing microwave non-absorbing materials, often in a microwave hybrid heating configuration, to achieve coupling of microwaves with non-microwave absorbing materials [14]. In addition to its microwave processing capabilities, the excellent mechanical and thermal characteristics of SiC and its ability to function in extreme environments [15,16] position it as a promising material for various applications including advanced electronic devices for power electronics, cladding material in light water reactors, photonics bridging quantum technologies [17] and energy applications [18], sensors, biosensors [16,19] and quantum sensor [20]. These applications are significantly affected by the presence of internal and extrinsic imperfections inside the SiC crystal. Vacancy point defects are the most studied defects to reduce their concentration or, in some cases, to control their concentrations by deliberately irradiating the pure material with accelerated ions or electrons or laser to control the formation from a single vacancy to an ensemble of them [21]. Furthermore, it is a well-known fact that no material is entirely devoid of defects (i.e. flawless) in the real world; some concentration of vacancies invariably exists within a crystal structure. Investigating

the impact of vacancy defects on the thermal and structural properties of 3C-SiC during its heating poses a considerable experimental challenge. Fortunately, recent advancements in computational and characterisation techniques have made it feasible to theoretically analyse thermal and structural properties at the atomic level [22]. Atomistic-level modelling techniques such as molecular dynamics have emerged as viable tools for simulating 3C-SiC with various concentrations of defects during microwave irradiation. Several computational studies have already reported on the impact of vacancies on the thermal and mechanical properties of 3C-SiC [23–25]. Li et al. [26] reported that while point defects had minimal impact on heat capacity and thermal expansion coefficient, the presence of vacancies in 3C-SiC led to a significant decrease in thermal conductivity. This reduction in thermal conductivity with increasing vacancy concentration was primarily attributed to the predominant mechanism of defect scattering of phonons. Samolyuk et al. [27] investigated the impact of single vacancies and microvoids on the thermal properties of 3C-SiC through a molecular dynamics approach. It was reported that thermal conductivity decreased by five-fold as the vacancy concentration increased from 0 to 0.46%. On the other hand, Mao et al. [28] explored the effect of eight distinct types of point defects on the thermal behaviour of 3C-SiC at various temperatures. It was reported that there was a rapid decrease in thermal conductivity at low defect concentrations, which stabilised at higher concentrations. However, any study on microwave heating of vacancy-induced 3C-SiC systems was hardly reported.

In recent years, few studies have been reported on microwave heating characteristics of different materials using the atomistic simulation method. Most of these studies are primarily limited to organic compounds like water [29,30], polyacrylonitrile (PAN) [31], toluene [32], and epoxy resin [33]. A few handful studies have explored the microwave heating characteristics of ceramic materials. Nukano et al. [34] conducted directional microwave heating simulations of α-alumina (Al_2O_3) using molecular dynamics and concluded that the rapid melting of α-Al_2O_3 by microwave energy occurred due to the high anisotropic mobility of aluminum (Al) atoms. Another study compared the microwave heating profiles of two different SiC models [35]. It was reported that the microwave heating of the 3C-SiC slab is directionally dependent on the direction of microwave exposure, whereas the heating in bulk 3C-SiC is directionally independent of microwaves [35]. A numerical relationship between electrical field strengths and frequencies was developed while microwave heating the 3C-SiC system to forecast the thermal behaviour and phase changes possible in the material [36]. Limited literature availability on microwave heating of 3C-SiC provides a scope to study the influence of vacancy defects on the thermal and structural properties of 3C-SiC at the molecular level during microwave exposure. In this work, a molecular dynamics-based approach has been used to investigate the effects of pre-existing Silicon (Si) vacancies in microwave heating of the 3C-SiC system. Thermal and microstructural evolution of the 3C-SiC system during microwave exposure has been analysed using mean square displacement (MSD) and diffusion coefficient.

Further, properties related to structural changes were examined in detail using the radial distribution function (RDF) and the identified diamond structure (IDS) modules in OVITO. Moreover, the influence of Si vacancy and C-vacancy was studied, and a comparative analysis has been presented for heating rate.

2 Computational methodology

In this work, three different models of the 3C-SiC system, including pristine, Si-vacancy and C-vacancy, have been used to study the microwave heating characteristics of the 3C-SiC system. In this section, model development and simulation strategy are discussed.

2.1 Pristine model

2.1.1 Model development

The pristine model of 3C-SiC was developed by considering the bond dynamics and interatomic interactions between Si and C atoms. The study implemented a three-body Vashishta interatomic potential proposed by Vashishta et al. [37]. The effectiveness of this potential has been previously demonstrated through accurate predictions of dislocation behaviour [38–40], diffusion behaviour [41], and microwave irradiation in SiC systems [35].

A periodic pristine 3C-SiC structure was constructed using ATOMSK platform [42]. The pristine 3C-SiC model has a dimension of 8.72×8.72×8.72 nm^3, consists of 64000 atoms residing in a zinc-blende structure.

2.1.2 Model validation

Simulations were conducted using the open-source Large-scale Atomic/Molecular Massively Parallel Simulator (LAMMPS) platform provided by Sandia National Laboratories (USA) [43]. Analysis of atomic configurations, structural changes, and post-processing of simulation results was conducted using the open visualisation tool (OVITO) software [44]. The pristine model was validated by comparing experimental XRD results with the simulated XRD profile (Fig. 1). The XRD analysis of pristine structure was carried on a Bruker D2 Phaser with Cu-Kα X-ray at a scanning rate of 1º min^{-1}. The XRD patterns of the pristine 3C-SiC were obtained before (Fig. 1(a)) and after microwave exposure (Fig. 1(b)), as illustrated in Fig. 1. Fig. 1(a) displays the XRD pattern of pristine 3C-SiC prior to microwave exposure. At the same time, Fig. 1(b) exhibits the XRD pattern after exposure to microwave energy (at 900 ºC). From the experimental study, the (101), (111), (103), (200), (220), (311) and (222) crystallographic planes for 3C-SiC were detected at scattering angles of 33.52º,35.53º , 37.86º, 40.88º, 59.44º, 71.28º and 74.8º, respectively.

In the simulation study, five peaks were identified at scattering angles of 35.76º, 41.52 º, 60.08º, 72.24º, and 75.44º, corresponding to (111), (200), (220), (311), and (222)

planes, respectively. The XRD pattern observed in the simulation study before microwave exposure closely resembled the experimental results depicted in Fig. 1(a). A similar trend was also seen in previous XRD studies on 3C-SiC conducted at room temperature [45,46]. Upon application of microwave energy, the system's temperature began to rise. Subsequently, the heights of the (111), (220), and (222) peaks decreased, and these peaks became broader and flatter, as depicted in Fig. 1(b). These changes in peaks confirm the heating of 3C-SiC structures via microwave energy. This study indicates that the developed model and simulation results for the pristine 3C-SiC structure agree well with the literature and experimental results. Therefore, the pristine model was used further to develop the vacancy-based models.

Fig. 1 The XRD patterns of pristine 3C-SiC during experimental and simulation studies in conditions (a) before MW exposure and (b) After MW exposure.

2.2 Vacancy-based Models

The initial computational model (i.e. pristine 3C-SiC) was obtained using the above-mentioned approach. To generate varying percentages of Si vacancies, n_i atoms were randomly eliminated from the original model. The selection of vacancy concentration was completely based on the available literature on MD study of 3C-SiC [23,27,47–49]. The percentage of vacancy and their corresponding atoms are detailed in Table 1. All simulation models were constructed using the ATOMSK software [42], maintaining a lattice constant of 4.36Å and adopting a zinc-blende structure. Fig. 2 depicts the initial configuration of the vacancy-induced 3C-SiC model, including its dimensions. In-plane periodic boundary conditions were applied from all the three directions to ease the impact of unbound edges. The C-vacancy based model was developed using the similar approach as a model was developed for Si vacancy. The details of the model are given in Table 1.

Fig. 2 A schematic representation of generated Si-vacancy induced 3C-SiC structure (simulation box size: 87.2×87.2×87.2 Å^3) and microwave (MW) heating of the structure along x-direction

Table 1: Si-vacancy and C-vacancy concentration of 3C-SiC structure

Model Attributes	**Type of vacancy**							
	Si-vacancy				C-vacancy			
Vacancy concentration (%)	0.5	1.0	1.5	2.0	0.5	1.0	1.5	2.0
No. of atoms removed (n_i)	160	320	480	640	160	320	480	640

2.3 Simulation

The initial equilibrium configuration of Si/C vacancy-induced 3C-SiC is attained by conducting system energy minimization through the conjugate gradient (CG)

algorithm [50,51]. This is performed in the LAMMPS software using the command “min_style” and “”minimize”. Thereafter, all the energy minimized model is equilibrated at 300 K with the help of canonical NVT ensemble [52,53] for 1.5 ns with a time step 1 fs. After relaxation of the system, the external alternating electric field with sine waveform was applied in x-direction in an microcanonical NVE ensemble to produce the microwave heating effect with amplitude of 0.1 and 0.5 V/Å. The associated alternating electric field can be expressed as follow [54]:

$$\vec{E} = E_x \sin(\omega t)$$

where, E_x is electric field strength or the amplitude applied in x-direction, ω is the angular frequency expressed as $2\pi f$, f is the frequency and t is the elapsed time for microwave exposure. The external electric field was applied to the system using the “fix efield” command provided in LAMMPS package, which will add a force of $F = qE$ to each charged atom [55,56]. Since 3C-SiC is non-magnetic in nature, it absorbs the electric field of microwave energy for heating. Frequency of the microwave considered for this study ranges from 100 to 300 GHz at an interval of 50 GHz. During the study, microwave irradiation on all the system was carried out for 5 ns. An individual charge of 1.201 and -1.201 was assigned to Si and C atoms respectively before applying the electric field [35,37].

Atomic motion within the system during microwave exposure was analysed in terms of MSD, which is commonly referred to as the extent of particle movement over time [57,58].

$$MSD(t) = \frac{1}{N}\sum_{i=1}^{N}\left|\overrightarrow{r_i}(t) - \overrightarrow{r_i}(0)\right|^2 \quad (2)$$

The self-diffusion coefficient (D) of the microwave-exposed 3C-SiC system was calculated from the slope of the MSD versus time data using the Einstein equation as follows [59]:

$$D = \frac{1}{6N}\lim_{t\to\infty}\sum_{i=1}^{N}\left|\overrightarrow{r_i}(t) - \overrightarrow{r_i}(0)\right|^2 \quad (3)$$

where N represents the number of atoms, r_i represents the position vector of *i*th particle and *t* represents the simulation time.

Structural changes during the microwave irradiation of Si/C vacancy induced 3C-SiC was measured utilizing the RDF, which can be expressed as [60,61]:

$$g_{\alpha\beta}(r) =$$

$$\frac{L^3}{N_\alpha N_\beta} \sum_{i=1}^{N} \frac{n_{i\beta}(r)}{4\pi r^2 \Delta r}$$

where α and β are the two kinds of atoms in the system, and N_α and N_β are the respective numbers of α and β, respectively. $n_{i\beta}(r)$ is the number of β with the radial of $r \rightarrow r + \Delta r$, which is centered on the ith atom of α. The average probability of finding the particle β at the distance r from α is denoted by $g_{\alpha\beta}(r)$, with a considered as the origin of coordinates.

3 Results and discussion

Molecular Dynamics simulations of MW heating of 3C-SiC models containing varying percentages of Si vacancies, ranging from 0.5 to 2.0%, were conducted. The results obtained are discussed in this section.

3.1 Analysis on Si vacancy-induced 3C-SiC

3.1.1 Evolution of temperature

The temperature evolution with time is illustrated in Fig. 3 under different electric field strengths (0.1 and 0.5 V/Å) and frequencies (100 – 300 GHz). It is evident from Fig. 3(a – d) that the temperature remains relatively stable across all systems under an electric field strength of 0.1 V/Å. It is apparent that higher the frequency and the electric field strength, the rise in temperature is higher in all cases. However, upon increasing the electric field strength from 0.1 to 0.5 V/Å at 300 GHz, a significant rise

in temperature can be observed, particularly in the 3C-SiC structures which have 1.5% and 2.0% Si vacancy. In the presence of an electric field strength of 0.5 V/Å and a frequency of 300 GHz, the 1.5% and 2.0% Si vacancy-containing structures reached their respective melting points at 4.985 and 4.5 nanoseconds, respectively. A similar temperature evolution pattern was observed in the pristine 3C-SiC system when microwave irradiated at 0.5 V/Å and 300 GHz [36]. It is worth noting that the Si vacancy-induced 3C-SiC system reaches the melting point of 3300 K at 0.3% and 10.2% early for 1.5% and 2% Si vacancy-induced 3C-SiC system, respectively as compared to the pristine system. Furthermore, the frequency at which the Si vacancy-induced 3C-SiC system reached the melting point was approximately 40% lower than pristine system. Further discussion on the increase in temperature and the associated phase change was conducted in subsequent sections of the study.

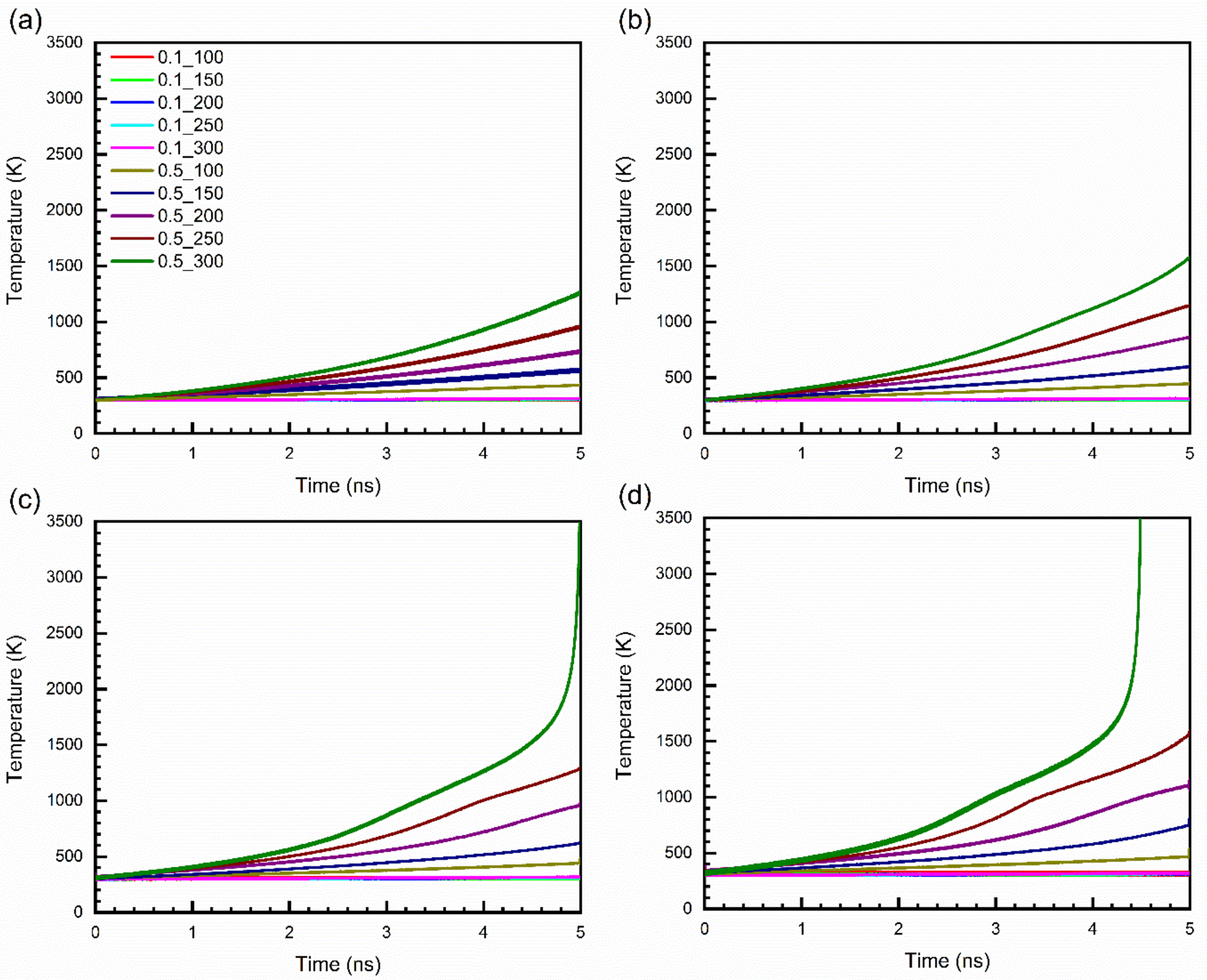

Fig. 3 Variation of temperature with time during microwave heating of 3C-SiC at different electric field strengths (V/Å) and frequencies (GHz) while varying Si vacancy concentrations (a) 0.5% (b) 1% (c) 1.5% and (d) 2.0%.

3.1.2 Microstructural evolution

A comprehensive depiction of atomic-level structural changes at an electric field strength of 0.5 V/Å and frequencies of 300 GHz for 1.5% and 2.0% Si vacancy-induced 3C-SiC structures is presented in Fig. 4(a-b). To facilitate a clearer understanding of the behaviour of defects and phase changes over time within the defect-induced

system during microwave irradiation, the structure was sliced from the middle using the OVITO platform.

Fig. 4 Snapshots of atomic-level structural analysis of Si-vacancy induced 3C-SiC structure during microwave exposure at Si vacancy concentrations (a) 1.5% and (b) 2.0 %.

For a Si-vacancy concentration of 1.5% (Fig. 4(a)), a slight movement of vacancies was observed until 3.0 ns during microwave exposure. At 4.5 ns, some vacancies were accumulated within the system and some of the cubic diamond structures got converted to cubic diamond (1st neighbour) and cubic diamond (2nd neighbour) structures. With further increase in microwave exposure time (at 4.985 ns), a sharp increase in vacancy concentration was observed and approximately 30.1% and 8.8% of atoms converted to cubic diamond (1st neighbour) and cubic diamond (2nd neighbour) structures, respectively.

For the 2.0% Si-vacancy concentration (Fig. 4(b)), a similar movement of atoms was observed until 3.0 ns, but the atom mobility was notably unstable and intense. This instability might account for the higher diffusion of atoms at this point. As microwave exposure continues till 4.49 ns, a sharp rise in temperature occurred (as observed in Fig. 3) and only 50% of the cubic diamond structure remained in the system, while the rest consisted of cubic diamond (1st neighbour), cubic diamond (2nd neighbour), and other structures. Further microwave exposure up to 4.5 ns, the Si-vacancy induced system had completely lost its crystallinity and converted into a liquid structure.

The abrupt phase structure transition occurring at 4.985 ns and 4.49 ns for 1.5% and 2.0% Si-vacancy 3C-SiC could account for the considerable temperature escalation during microwave exposure. This temperature surge in these structures surpasses that of pristine 3C-SiC, indicating a pronounced influence of defects on the temperature rise. Previous studies have indicated that the presence of defects enhances microwave absorption efficiency by inducing a thermal shock effect in the material [62]. The primary mechanism that drives the microwave absorption involves either the generation of frictional heating or the induction of eddy currents within the system [62]. Additionally, the rise in temperature in defect-induced 3C-SiC may be due to the excitation of non-thermal phonons and localized resonant coupling of point defects [63].

3.1.3 Radial distribution function

The pre-existing vacancy, along with the electric field strength and frequency, undoubtedly influence the intricate temperature elevation in 3C-SiC during microwave exposure. To comprehend the structural alterations, the Radial Distribution Function (RDF) of the Si vacancy-induced 3C-SiC system before and after exposure to the microwave field was computed and depicted in Fig. 5(a-b). The RDF plots obtained after equilibration with various vacancy percentages are illustrated in Fig. 5(a). Each plot exhibits a distinct peak at the equilibration point, indicating that the system maintained its bulk crystalline order and the structure is stable. Following microwave exposure for 1 ns, a slight decline in the Si-C peak was noted, as depicted from Supplementary Fig. S1. As the electric field strength and frequency increase, the first peak tends to reduce. It is evident from the figures that the elevation of the peaks decreases with an increase in vacancy percentage. It is obvious to compute and analyse RDF at vacancy concentrations 1.5% and 2.0% in Si vacancy-induced 3C-SiC during microwave exposure as a sharp increase in temperature occurs in these concentrations at 0.5 V/Å and 300 GHz (Fig. 3 (c–d)). The RDF was computed and plotted as depicted in Fig. 5(b). At an electric field strength of 0.1 V/Å, each RDF peak appears sharp and relatively higher, similar to the RDF peak observed in Fig. S1. However, when the electric field strength increases to 0.5 V/Å, the peaks begin to weaken in terms of intensity. Moreover, the length of the peak decreases and the width increases with the rise in frequency at 0.5 V/Å. The peak shifting towards a straight line at higher electric field strengths and frequencies confirms that the system is

approaching its melting point. This decrease in peak intensity mainly attributed to the structural changes occurring within the system and its decrease in crystallinity, since the system is moving towards melting region [64].

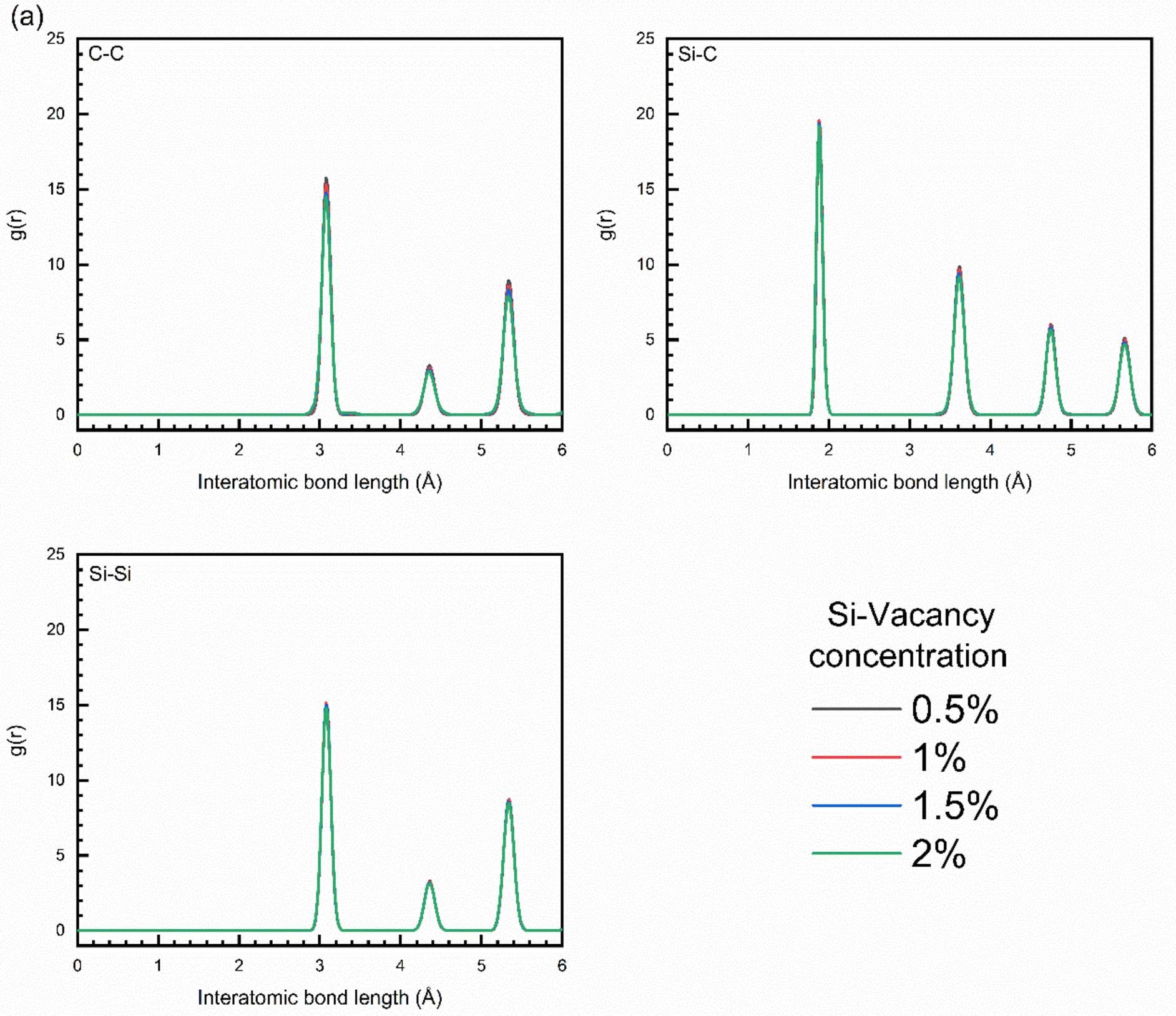

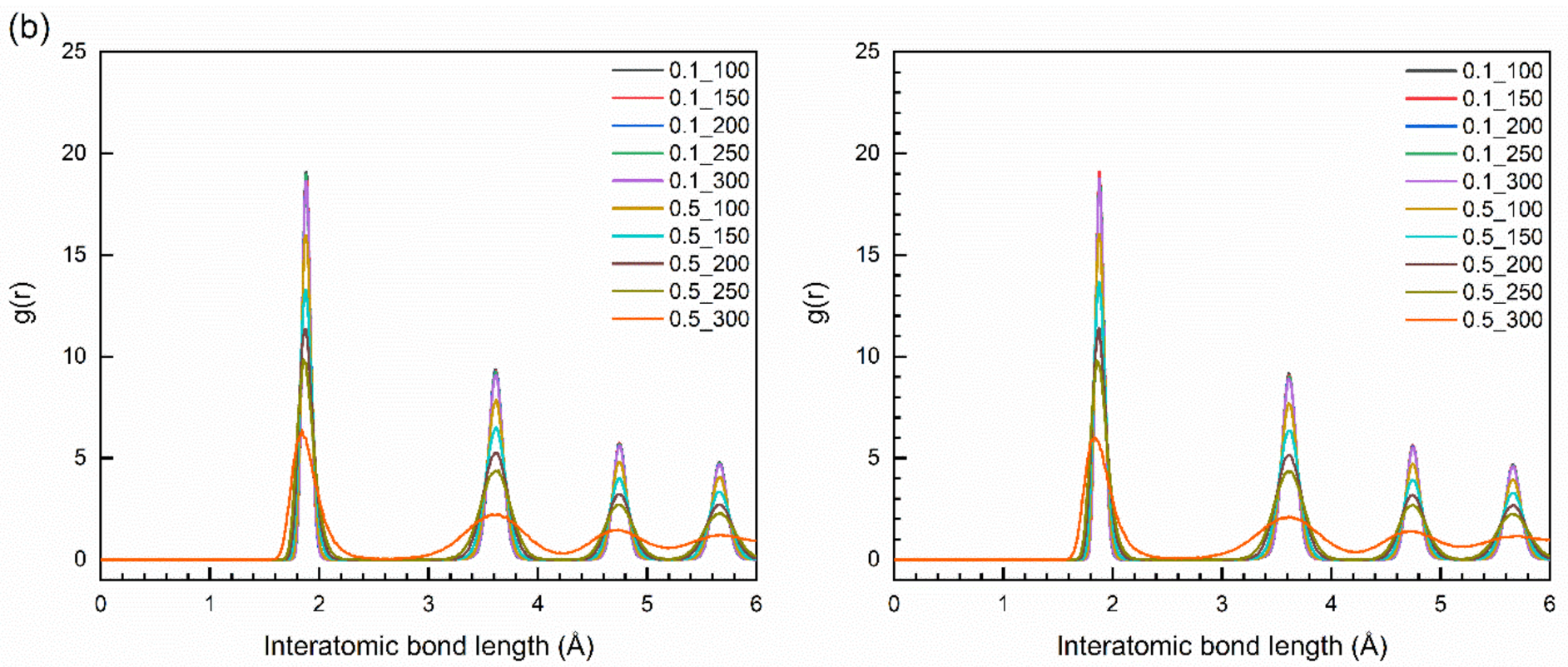

Fig. 5 RDF plots of Si-vacancy induced 3C-SiC during microwave irradiation (a) at equilibration point and (b) at 4.985 ns and 4.49 ns for 1.5% and 2.0% Si-vacancy respectively (Si-C)

3.1.4 Mean square displacement and diffusion coefficient

Fig. 6(a-d) illustrates the MSD of the microwave-irradiated Si vacancy-induced 3C-SiC system. Qualitatively, the MSD plots (Fig. 6) for different Si vacancies exhibit similar trends as observed in the case of temperature variation (Fig. 3). It is evident from Fig. 6 that the MSD value increases with an increase in vacancy concentration. This finding is consistent with previous literature on Si clusters with varying percentages of vacancy defects [65]. For 0.5% and 1.0% of Si vacancy, the MSD values remained almost constant over time, indicating minimal surface disorder within the system, maintaining a solid state. However, with an increase in Si vacancy concentration, particularly at an electric field strength of 0.5 V/Å and a frequency of 300 GHz, a sudden rise in MSD value was observed just after 4 ns. This abrupt increase in MSD values is primarily attributed to the formation of a liquid phase or surface disorder within the system. Additionally, the system undergoes a first-order melting transition, where the crystallinity of the system begins to collapse.

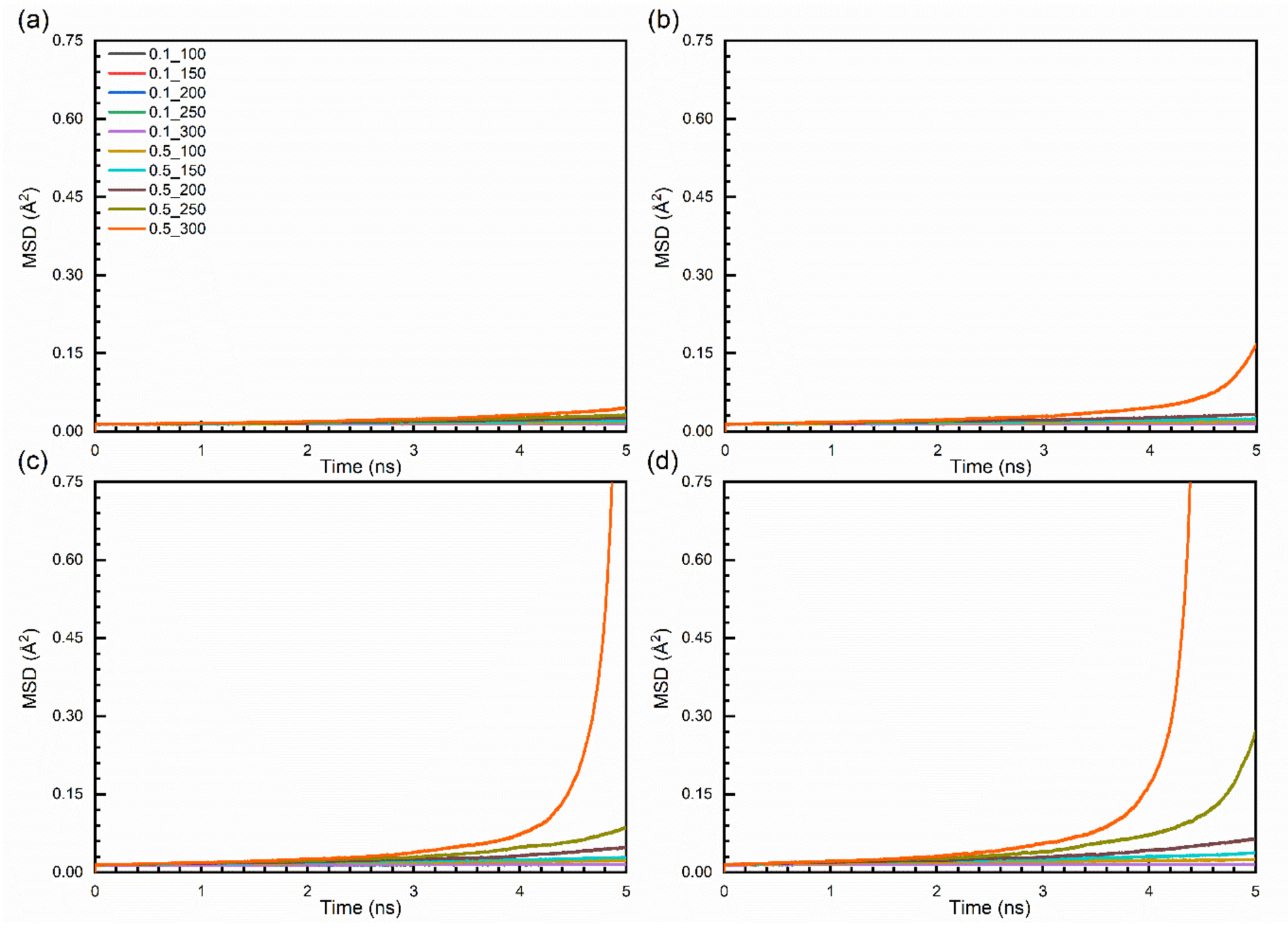

Fig. 6 Mean squared displacement (MSD) of Si-vacancy induced 3C-SiC system during microwave irradiation at vacancy concentrations (a) 0.5%, (b) 1%, (c) 1.5% and (d) 2.0%.

The diffusion coefficient obtained at an electric field strength of 0.5 V/Å and at a frequency of 300 GHz for the 3C-SiC system with different vacancy concentrations were calculated and presented in Fig. 7. Until 2 ns, the temperature and MSD variation for 0.5 V/Å at 300 GHz, was almost linear for the all the vacancy concentration. The slope of the MSD curve during this time interval was measured and plotted in Fig. 5. The diffusion coefficient of the Si vacancy-induced 3C-SiC increases with an increase in vacancy concentration during microwave irradiation. The diffusion coefficient obtained at 2.0% Si vacancy, was around approximately 195%, 90.4% and 15.59% higher than 0.5, 1.0 and 1.5% Si vacancy concentration respectively. This increase in

diffusion is mainly attributed to the amount of point defect concentrations and their mobility inside the 3C-SiC system [63].

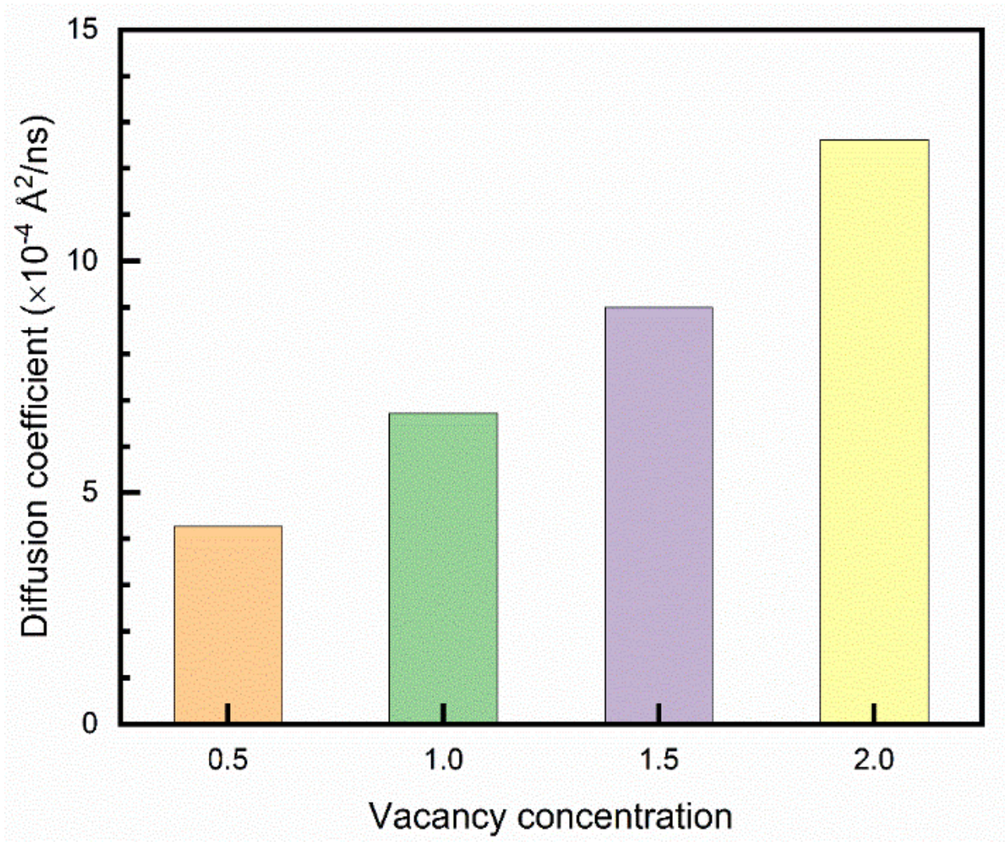

Fig. 7 Diffusion coefficient of Si-vacancy induced 3C-SiC system during microwave irradiation at 0.5 V/Å and 300 GHz.

3.1.5 Evolution of Si vacancies during microwave irradiation

The significant temperature elevation was observed in 3C-SiC systems with 1.5% and 2.0% Si-vacancy at high electric field strengths (0.5 V/Å) and frequencies (250 and 300 GHz) as evident from Fig. 3. Therefore, in this section, the study is focused on the evaluation of vacancy concentrations 1.5% and 2.0% and Figs. 8(a-b) illustrate the evolution of the distribution of Si vacancies at specific time intervals during microwave exposure, while the results for the remaining cases have been presented in

the supplementary Fig. S2. The microwave heating effect was studies on two specific Si-vacancies, V_1 and V_2 (Fig. 8) for 1.5% and 2.0% Si-vacancy. Initially (at t=0 ns), both Si-vacancies were surrounded by four C-atoms, occupying the cubic diamond (2^{nd} neighbour) phase, while these C-atoms were further encircled by 8 Si-atoms in the cubic diamond (1^{st} neighbour) phase. In case of 1.5% Si-vacancy at 250 GHz and 300 GHz, vacancies move within the system without altering the structure up to time span of 4.5 ns as depicted in Fig. 8(a). Once the temperature reaches 1200 K at 4.61 ns (at 250 GHz) and 4.5 ns (at 300 GHz), the vacancies began to diffuse within the system. It results in the transition of almost all carbon atoms to Cubic diamond from the cubic diamond (2^{nd} neighbour) phase. It was observed that an increase in microwave exposure time results in a decrease in the size of the vacancy. Subsequently, as the microwave exposure time increased (especially at 300 GHz frequency), nearing the melting region, the atoms began to displace from their original positions, ultimately transforming into amorphous (other) structures (Fig. 8(a)). Similar phenomena were also observed in the case of 2.0% Si-vacancy (Fig. 8(b)); however, the diffusion of vacancies occurred before 4.5 ns during microwave exposure as compared to the 1.5% Si-vacancy. In this case also, the diffusion of vacancies started beyond 1200 K which was attained at 3.91 ns and 3.77 ns for 250 GHz and 300 GHz, respectively. Further, increase in microwave exposure time results in the breaking of the bonds and movement of atoms from their initial position due to increase in system temperature. In a previous experimental study on SiC, it was reported that there was no alteration in

the type of vacancy defects at annealing temperatures up to 873 K. However, vacancies began to anneal out when the temperature exceeded 1273 K [66]. A similar annealing behaviour of vacancies was observed during migration studies of vacancies at higher temperatures [67]. The migration of Si-vacancies is evident in this study and it is in good agreement with the previous report [59].

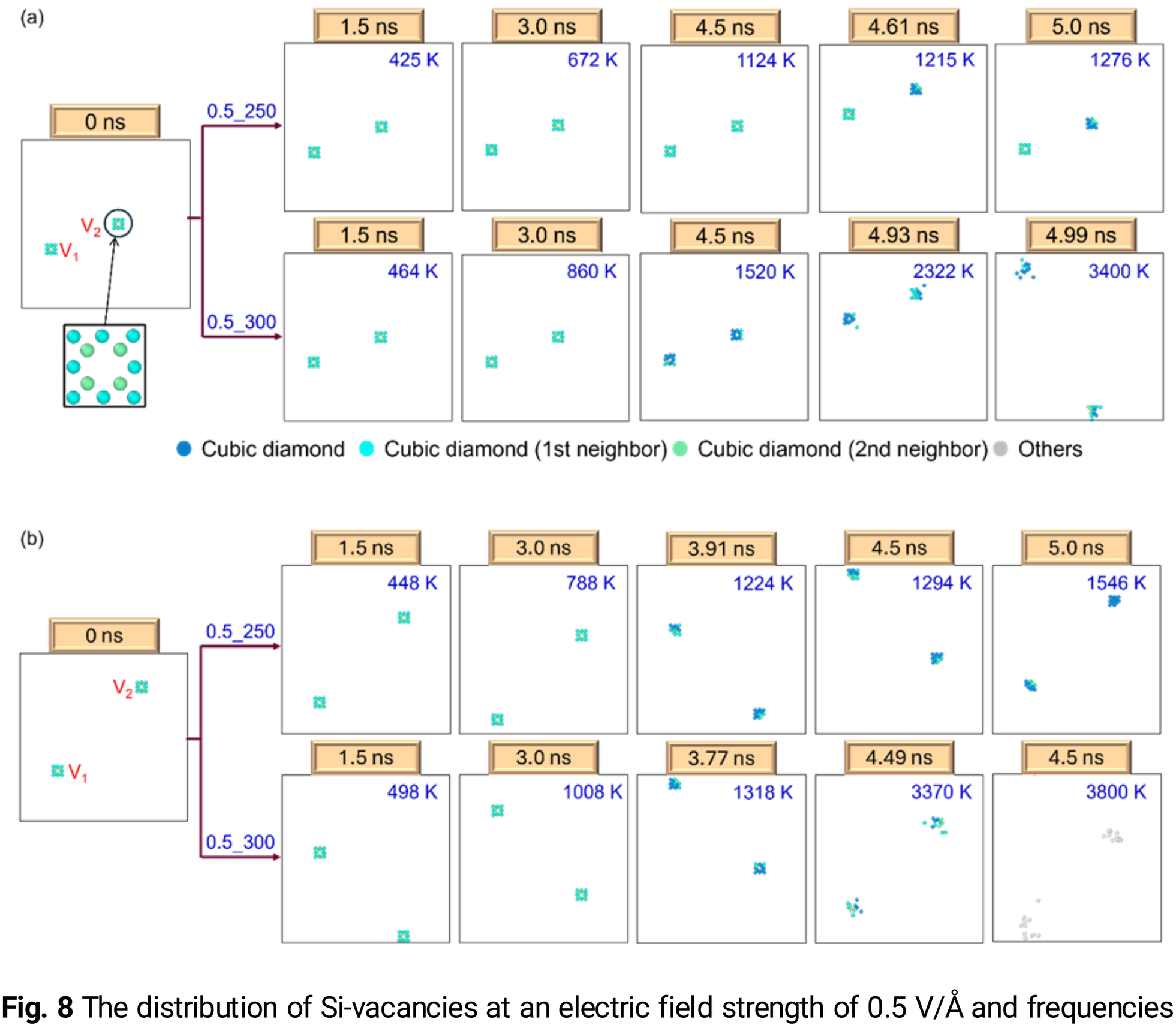

Fig. 8 The distribution of Si-vacancies at an electric field strength of 0.5 V/Å and frequencies 250 GHz and 300 GHz for (a) 1.5% Si-vacancy and (b) 2.0% Si-vacancy.

3.2 Analysis of C and Si vacancies induced 3C-SiC systems

Interaction of microwaves with 3C-SiC systems having different concentrations of C and Si vacancies (0.5%, 1.0%, 1.5%, and 2.0%) was studies for 1.5 ns at 0.5 V/Å and frequencies 100 GHz, 150 GHz, 200 GHz, 250 GHz, and 300 GHz (Fig. 9(a)). It is evident from Fig. 9(a) that up to 1.5 ns of microwave exposure, all the Si-vacancy induced system exhibits approximately linear relationship of temperature variation with frequency and the evolved temperature for C-vacancies remain higher than Si-vacancies for all frequencies. In case of 3C-SiC with lower C-vacancy percentages (0.5%, and 1.0%), the temperature varies linearly with frequency, whereas, for the C-vacancy concentrations 1.5% and 2.0%, the temperature maintains a linear relationship with frequency up to 200 GHz and the structure attains 607 K (1.5% C-vacancy) and 779 K (2.0 % C-vacancy). Beyond 200 GHz, a rapid increase in temperature of C-vacancy concentrations 1.5% and 2.0% was observed for higher frequencies like 250 GHz and 300 GHz.

Further, to understand the microwave heating behaviour of both the vacancies in 3C-SiC system, the thermal-conductivity 2.0% C vacancy and 2.0% Si vacancy induced 3C-SiC systems was analysed and compared with the thermal-conductivity of pristine 3C-SiC structure using the non-equilibrium molecular dynamics (NEMD) simulation. The obtained results for thermal conductivities for 3C-SiC system having no vacancy, 2.0% C vacancy and 2.0% Si vacancy were plotted as a function of temperature as shown in Fig. 9(b). It is indicated by Fig. 9(b) that the thermal conductivity of pristine 3C-SiC is higher as compared to vacancy induced systems, which is in agreement with

the previous studies [25,26]. Thermal conductivity shows a rapid increase for all the 3C-SiC systems up to 500K, thereafter, it decreases with increase in temperature for all systems. It can be concluded from Fig. 9(b) that the thermal conductivity plays a significant role in increase in temperature till 1000 K during microwave exposure. The Si and C-vacancies induced 3C-SiC system exhibit almost similar trend of thermal conductivity beyond 1000 K. However, the temperature evolution in C-vacancy induced 3C-SiC is significant as compared to Si-vacancy 3C-SiC system. Reasons for such microwave heating behaviour have been discussed in subsequent section.

Fig.9 (a) Variation of temperature with frequency during microwave irradiation at 0.5 V/Å electric field strength (b) Calculated thermal conductivity with respect to temperature for pristine, 2.0% Si-vacancy and 2.0% C-vacancy induced 3C-SiC system.

A significant evolution of temperature was demonstrated by 3C-SiC systems containing C vacancies (1.5% and 2.0%) during microwave exposure (Fig. 9(a)). Therefore, the microwave heating behaviour of 3C-SiC system was further analysed for 3C-SiC

structures containing 1.5% and 2.0% of Si and C vacancies at 0.5 V/Å and various frequencies (100 to 300 GHz). The obtained results for temperature evolution are shown in Figs. 10 (a-d). In both the cases of C and Si vacancies, the 2.0% vacancy offers higher temperature evolution during microwave exposure than 1.5% vacancy. Additionally, C-vacancy enhances temperature evolution as compared to Si-vacancy. The Si-vacancy induces heating rates of 91.2 Kns^{-1}, 145.8 Kns^{-1}, 213.4 Kns^{-1}, 309.1 Kns^{-1}, and 750.2 Kns^{-1} at frequencies 100 GHz, 150 GHz, 200 GHz, 250 GHz and 300 GHz, respectively. It is evident from Fig. 10 that the presence of C-vacancy enhances the rate of microwave heating of the 3C-SiC system as compared to Si-vacancy at each frequency approximately beyond 1 ns. For example, at a frequency of 300 GHz, the time taken to reach the melting point for 1.5% and 2.0% C-vacancy-induced 3C-SiC was approximately half that of the Si-vacancy-induced 3C-SiC system. Moreover, the C-vacancy induces 221.8%, 489.0%, 425.0%, 361.2%, and 142.3% higher heating rates at frequencies 100 GHz, 150 GHz, 200 GHz, 250 GHz and 300 GHz, respectively as compared to Si-vacancy based systems.

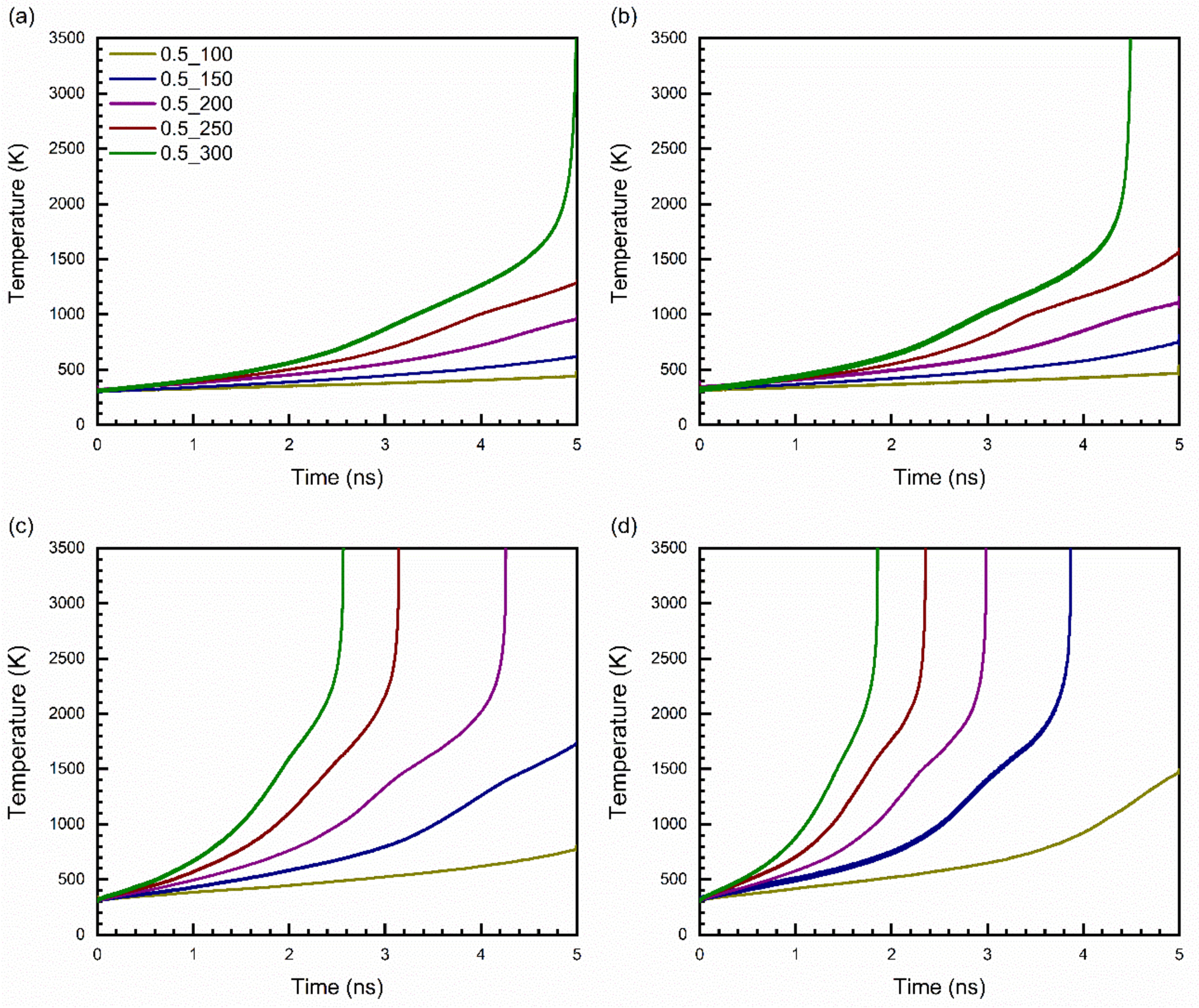

Fig. 10 Variation of temperature with time during microwave heating of 3C-SiC at different vacancy concentrations (a) 1.5% Si (b) 2.0% Si (c) 1.5% C and (d) 2.0% C at 0.5 V/Å and different frequencies ranging from 100 to 300 GHz (indicated by colours in the legend).

The temperature increase beyond 1000 K during microwave exposure of all the 3C-SiC systems was further analysed using mean square displacement (MSD) and diffusion coefficient. The MSD plots at 0.5 V/Å and 300 GHz are shown in Fig. 11(a) for pristine, 1.5% and 2.0% C and Si-vacancies induced 3C-SiC. Variation in diffusion coefficient of 1.5% and 2.0% C and Si-vacancies induced 3C-SiC systems is depicted in Fig. 11(b) at different frequencies. For pristine 3C-SiC, it was reported that temperature reaches up

to 550 K during microwave exposure for 5 ns at 0.5 V/Å and 300 GHz [36]. Consequently, the MSD of pristine 3C-SiC is almost linear over the period of microwave exposure as shown in Fig. 11(a). It is evident from Fig. 11(a) that with the introduction of vacancies, the particle mobility enhanced significantly especially for C-vacancy induced 3C-SiC up to 0.66 $Å^2$ and 0.75 $Å^2$ at 1.5% and 2% vacancies, respectively. On the other hand, Si-vacancy of 1.5% and 2.0% could reach 0.024 $Å^2$ and 0.029 $Å^2$ respectively in similar time of microwave exposure. In case of 2.0% Si-vacancy, the mobility of particle is linear until 3.5 ns of microwave exposure time i.e. at 1000 K (also depicted in Fig. 3) then a sudden increment was noticed. Similar behaviour can be observed in other cases of vacancies. Previous studies have reported higher mobility of C-antisites than Si-antisites [67]. This was further verified though diffusion coefficient analysis (Fig. 11(b)) for the vacancy induced system. It is indicted by Fig. 11(b) that the diffusivity of C-vacancy induced 3C-SiC systems are higher than the corresponding Si-vacancy induced 3C-SiC systems. The 2.0% C-vacancy induced 3C-SiC system have 83.9%, 87.1%, 158.5%, 195.3%, and 386.4%, higher diffusion coefficient value than 2.0% Si-vacancy induced 3C-SiC system at 100 GHz, 150 GHz, 200 GHz, 250 GHz, and 300 GHz, respectively. It can be concluded that the C-vacancy provides scopes for higher diffusion of atoms during microwave heating.

Fig. 11 (a) Particle mobility during microwave exposure at an electric field strength of 0.5 V/Å and frequency of 300 GHz (b) Diffusion coefficient of 1.5% and 2.0% Si and C-vacancy at 0.5 V/Å electric field strength and different frequencies

It can be concluded from previous section that C- vacancy expedites the microwave heating of 3C-SiC systems as compared to Si-vacancy at 0.5 V/Å and 300 GHz. The rapid heating behaviour of 2.0% C and Si-vacancies behaviour was further analysed to understand the atomic structural changes that occur during microwave exposure. Fig. 12(a) shows time-temperature profile of 3C-SiC system having 2.0% Si and 2.0% C vacancies. The atomic structural changes for 2.0% Si (indicated by points A, B, and C in Fig. 12(a)) and 2%C (indicated by points A^1, B^1, and C^1 in Fig. 12(a)) vacancies are presented in Fig. 12(b) and 12(c), respectively. Up to 1 ns, all the atoms in the vacancy remains intact to their position (as indicated by point A in Fig. 12(b) and A^1 in Fig. 12(c)). Once the microwave exposure time reaches at 1.4 ns, i.e. at point B (Fig. 12(b)), one of the Si atoms from the Si-vacancy moves out from its position; consequently, the structure transits from a cubic diamond (2^{nd} neighbour) phase to an amorphous

structure. On the contrary, at the point B^1 (Fig. 12(c)), no transition behaviour was observed for C-vacancy. With further microwave exposure up to 1.85 nanoseconds, the structure containing Si-vacancy remains in in a state (C in Fig. 12(b)) similar to 1.4 ns state (B in Fig. 12(b)), whereas, atoms within the C-vacancy structure showed transition to an amorphous phase (C^1 in Fig. 12(c)) due to achieving their melting point. It can be concluded from the discussion that microwave heating is driven by structural changes induced by vacancies in the 3C-SiC structures.

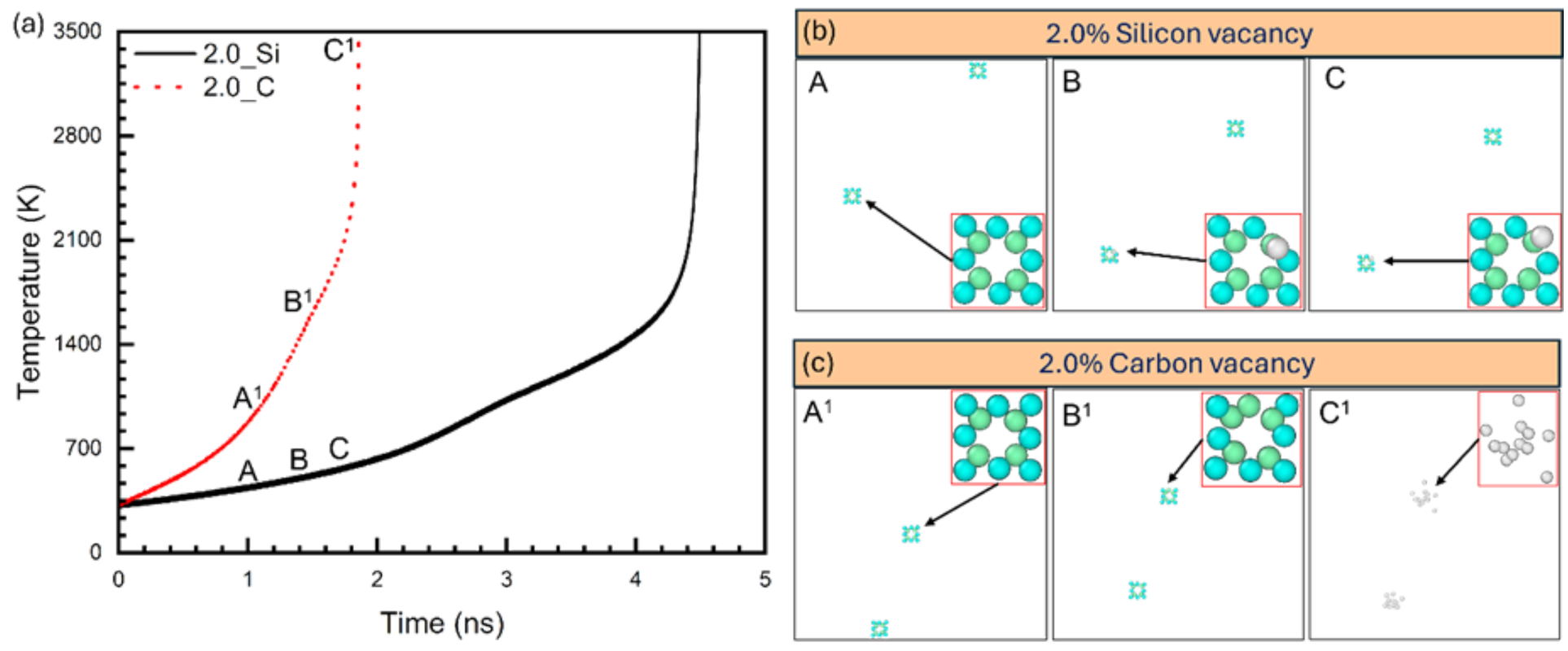

Fig.12 (a) Time-temperature profile for 3C-SiC system with 2.0% Si and 2.0% C vacancies during microwave exposure at 0.5 V/Å and 300 GHz, and atomic structural change for (b) 2.0% Si-vacancy at points A, B and C indicated on temperature profile of 2% Si in Fig 12(a), and (c) 2.0% C-vacancy at points A^1, B^1 to C^1 indicated on temperature profile of 2% C in Fig 12(a).

4 Conclusion

Classical MD simulation was employed to investigate the impact of varying concentrations of Si vacancy defects on the thermal and physical behaviour of the

3C-SiC system under microwave exposure. Microwave heating was applied to the system at different electric field strengths (0.1 and 0.5 V/Å) and frequencies (100, 150, 200, 250, and 300 GHz). The following key findings emerged from the study:

- As the Si-vacancy concentration increased, the 3C-SiC system approached its melting point at a faster rate. The diffusivity at 2.0% Si was almost 195%, 90.4% and 15.59% higher than 0.5%, 1.0% and 1.5% Si vacancy.
- The RDF analysis indicates reduction in crystallinity by 66.67% and 72.22% for 1.5% and 2.0% Si-vacancy with the application of microwave energy. Loss in crystallinity is mainly attributed to the change in phase from cubic diamond to other (amorphous) structures at 0.5 V/Å and 300 GHz for both the vacancies.
- Annealing of Si-vacancy induced 3C-SiC starts at 900 K and at around 1500 K most of the Si-vacancy starts to anneal out. Annealing of Si-vacancy occurred at a lower temperature than the C-vacancy.
- IDS analysis revealed sharp change in phase for above mentioned vacancies at 4.985 ns and 4.49 ns, respectively. Additionally, the 2.0% Si-vacancy induced 3C-SiC system attained the melting point at just 4.5 ns of microwave exposure time.
- Heating in 3C-SiC with vacancy during microwave exposure occurred due to two mechanisms. At the initial phase thermal conductivity plays a major role in increase in temperature, later particle mobility helps to sudden increment in temperature.

- Compared to Si-vacancy, 2.0% C-vacancy exhibits a higher microwave heating rate of 221.8%, 489.0%, 425.0%, 361.2%, and 142.3% at 100 GHz, 150 GHz, 200 GHz, 250 GHz, and 300 GHz, respectively.

Declarations

Data Availability

The data that support the findings of this study are available from the corresponding author upon reasonable request.

Declaration of competing interest

The authors have no conflicts to disclose.

Acknowledgements

Saurav Goel would like to acknowledge the funding support from UKRI via Grant No. EP/T024607/1 and the International Exchange Cost Share award by the Royal Society (IEC\NSFC\223536). Additionally, we are grateful to be granted access to various HPC resources including the Isambard Bristol, UK supercomputing service as well as Kittrick (LSBU, UK) and Param Ishan (IIT Guwahati, India).

References

[1] D.E. Clark, W.H. Sutton, Microwave processing of materials, Annu. Rev. Mater. Sci. 26

(1996) 299–331. https://doi.org/10.1017/S0883769400038495.

[2] R.R. Mishra, A.K. Sharma, A Review of Research Trends in Microwave Processing of Metal-Based Materials and Opportunities in Microwave Metal Casting, Crit. Rev. Solid State Mater. Sci. 41 (2016) 217–255. https://doi.org/10.1080/10408436.2016.1142421.

[3] B. Sharma, S. Thakur, D. Trache, H.Y. Nezhad, V.K. Thakur, Microwave-assisted rapid synthesis of reduced graphene oxide-based gum tragacanth hydrogel nanocomposite for heavy metal ions adsorption, Nanomaterials. 10 (2020) 1–22. https://doi.org/10.3390/nano10081616.

[4] D. Li, J. Barrington, S. James, D. Ayre, M. Słoma, M.F. Lin, H. Yazdani Nezhad, Electromagnetic field controlled domain wall displacement for induced strain tailoring in BaTiO3-epoxy nanocomposite, Nature Publishing Group UK, 2022. https://doi.org/10.1038/s41598-022-11380-9.

[5] D. El Khaled, N. Novas, J.A. Gazquez, F. Manzano-Agugliaro, Microwave dielectric heating: Applications on metals processing, Renew. Sustain. Energy Rev. 82 (2018) 2880–2892. https://doi.org/10.1016/j.rser.2017.10.043.

[6] R.R. Mishra, A.K. Sharma, Microwave-material interaction phenomena: Heating mechanisms, challenges and opportunities in material processing, Compos. Part A Appl. Sci. Manuf. 81 (2016) 78–97. https://doi.org/10.1016/j.compositesa.2015.10.035.

[7] J. Sun, W. Wang, Q. Yue, Review on microwave-matter interaction fundamentals and efficient microwave-associated heating strategies, Materials (Basel). 9 (2016).

https://doi.org/10.3390/ma9040231.

[8] R. Krishnan, S.N. Shibu, D. Poelman, A.K. Badyal, A.K. Kunti, H.C. Swart, S.G. Menon, Recent advances in microwave synthesis for photoluminescence and photocatalysis, Mater. Today Commun. 32 (2022) 103890. https://doi.org/10.1016/j.mtcomm.2022.103890.

[9] C.O. Mgbemena, D. Li, M.F. Lin, P.D. Liddel, K.B. Katnam, V.T. Kumar, H.Y. Nezhad, Accelerated microwave curing of fibre-reinforced thermoset polymer composites for structural applications: A review of scientific challenges, Compos. Part A Appl. Sci. Manuf. 115 (2018) 88–103. https://doi.org/10.1016/j.compositesa.2018.09.012.

[10] W. Duan, X. Yin, Q. Li, X. Liu, L. Cheng, L. Zhang, Synthesis and microwave absorption properties of SiC nanowires reinforced SiOC ceramic, J. Eur. Ceram. Soc. 34 (2014) 257–266. https://doi.org/10.1016/j.jeurceramsoc.2013.08.029.

[11] X. Liu, J. Xue, F. Ren, F. Ye, X. Fan, Y. Liu, L. Cheng, Enhanced microwave-absorption properties of polymer-derived SiC/SiOC composite ceramics modified by carbon nanowires, Ceram. Int. 46 (2020) 20742–20750. https://doi.org/10.1016/j.ceramint.2020.05.018.

[12] S.C. Chiu, H.C. Yu, Y.Y. Li, High electromagnetic wave absorption performance of silicon carbide nanowires in the gigahertz range, J. Phys. Chem. C. 114 (2010) 1947–1952. https://doi.org/10.1021/jp905127t.

[13] W. Duan, X. Yin, C. Luo, J. Kong, F. Ye, H. Pan, Microwave-absorption properties of SiOC ceramics derived from novel hyperbranched ferrocene-containing polysiloxane, J. Eur. Ceram. Soc. 37 (2017) 2021–2030.

https://doi.org/10.1016/j.jeurceramsoc.2016.12.038.

[14] B. Yahaya, S. Izman, M. Konneh, N. Redzuan, Microwave Hybrid Heating of Materials Using Susceptors- A brief review, 845 (2014) 426–430. https://doi.org/10.4028/www.scientific.net/AMR.845.426.

[15] D. Varshney, S.S.M. Varshney, N.S.R. Khenata, Elastic and thermodynamical properties of cubic (3 C) silicon carbide under high pressure and high temperature, J. Theor. Appl. Phys. 9 (2015) 221–249. https://doi.org/10.1007/s40094-015-0183-7.

[16] F. La Via, D. Alquier, F. Giannazzo, T. Kimoto, P. Neudeck, H. Ou, A. Roncaglia, S.E. Saddow, S. Tudisco, Emerging SiC Applications beyond Power Electronic Devices, Micromachines. 14 (2023) 1–37. https://doi.org/https://doi.org/10.3390/mi14061200.

[17] S. Castelletto, A. Peruzzo, C. Bonato, B.C. Johnson, M. Radulaski, H. Ou, F. Kaiser, J. Wrachtrup, Silicon Carbide Photonics Bridging Quantum Technology, ACS Photonics. 9 (2022) 1434–1457. https://doi.org/10.1021/acsphotonics.1c01775.

[18] B.N. Pushpakaran, A.S. Subburaj, S.B. Bayne, J. Mookken, Impact of silicon carbide semiconductor technology in Photovoltaic Energy System, Renew. Sustain. Energy Rev. 55 (2016) 971–989. https://doi.org/10.1016/j.rser.2015.10.161.

[19] S.E. Saddow, Silicon Carbide Technology for Advanced Human Healthcare Applications, Micromachines. 13 (2022) 1–21. https://doi.org/https://doi.org/10.3390/mi13030346.

[20] S. Castelletto, C.T.K. Lew, W.X. Lin, J.S. Xu, Quantum systems in silicon carbide for sensing applications, Reports Prog. Phys. 87 (2024). https://doi.org/10.1088/1361-6633/ad10b3.

[21] Y. Fan, Z. Xu, Y. Song, T. Sun, Molecular dynamics simulation of silicon vacancy defects in silicon carbide by hydrogen ion implantation and subsequent annealing, Diam. Relat. Mater. 119 (2021) 108595. https://doi.org/10.1016/j.diamond.2021.108595.

[22] S. Daoud, N. Bouarissa, H. Rekab-djabri, P.K. Saini, Structural and Thermo-Physical Properties of 3C-SiC : High-Temperature and High-Pressure Effects, Silicon. 14 (2022) 6299–6309. https://doi.org/https://doi.org/10.1007/s12633-021-01387-8.

[23] Y. Li, Y. Li, W. Xiao, Point defects and grain boundary effects on tensile strength of 3C-SiC studied by molecular dynamics simulations, Nucl. Eng. Technol. 51 (2019) 769–775. https://doi.org/10.1016/j.net.2018.12.010.

[24] K. Ren, L. Huang, H. Shu, G. Zhang, W. Mu, H. Zhang, H. Qin, G. Zhang, Impacts of defects on the mechanical and thermal properties of SiC and GeC monolayers, Phys. Chem. Chem. Phys. 25 (2023) 32378–32386. https://doi.org/10.1039/d3cp04538b.

[25] A.S.M.J. Islam, M.S. Islam, N. Ferdous, J. Park, A. Hashimoto, Vacancy-induced thermal transport in two-dimensional silicon carbide: A reverse non-equilibrium molecular dynamics study, Phys. Chem. Chem. Phys. 22 (2020) 13592–13602. https://doi.org/10.1039/d0cp00990c.

[26] J. Li, L. Porter, S. Yip, Atomistic modeling of finite-temperature properties of crystalline b -SiC II. Thermal conductivity and effects of point defects, J. Nucl. Mater. 255 (1998) 139–152. https://doi.org/https://doi.org/10.1016/S0022-3115(98)00034-8.

[27] G.D. Samolyuk, S.I. Golubov, Y.N. Osetsky, R.E. Stoller, Molecular dynamics study of influence of vacancy types defects on thermal conductivity of β-SiC, J. Nucl. Mater. 418 (2011) 174–181. https://doi.org/10.1016/j.jnucmat.2011.06.036.

[28] Y. Mao, Y. Li, Y. Xiong, W. Xiao, Point defect effects on the thermal conductivity of β-SiC by molecular dynamics simulations, Comput. Mater. Sci. 152 (2018) 300–307. https://doi.org/10.1016/j.commatsci.2018.05.050.

[29] N.D. Afify, M.B. Sweatman, Classical molecular dynamics simulation of microwave heating of liquids: The case of water, J. Chem. Phys. 148 (2018). https://doi.org/10.1063/1.5001928.

[30] M. Tanaka, M. Sato, Microwave heating of water, ice, and saline solution: Molecular dynamics study, J. Chem. Phys. 126 (2007). https://doi.org/10.1063/1.2403870.

[31] C. Wang, H. Liu, L. Song, J. Tan, W. Yang, L. Cheng, Temperature evolution, atomistic hot-spot effects and thermal runaway during microwave heating of polyacrylonitrile: A ReaxFF molecular dynamics simulation, Nano Sel. 2 (2021) 2373–2379. https://doi.org/10.1002/nano.202100061.

[32] Y.M. Zhang, J.L. Li, X.Y. Wang, J.P. Wang, W. Shao, S.Q. Xiao, B.Z. Wang, Research on pyrolysis of toluene under microwave heating by using ReaxFF molecular dynamics simulations, Mol. Phys. 112 (2014) 1724–1730. https://doi.org/10.1080/00268976.2013.860245.

[33] Y.M. Zhang, J.L. Li, J.P. Wang, X.S. Yang, W. Shao, S.Q. Xiao, B.Z. Wang, Research on epoxy resin decomposition under microwave heating by using ReaxFF molecular dynamics simulations, RSC Adv. 4 (2014) 17083–17090. https://doi.org/10.1039/c4ra00473f.

[34] Y. Hu, A. Nakano, J. Wang, Directional melting of alumina via polarized microwave heating, Appl. Phys. Lett. 110 (2017). https://doi.org/10.1063/1.4973698.

[35] T.A. Khan, P.A. Burr, D. Payne, M. Juhl, U. Das, B. Hallam, D. Bagnall, B. Puthen Veettil, Molecular dynamic simulation on temperature evolution of SiC under directional microwave radiation, J. Phys. Condens. Matter. 34 (2022). https://doi.org/10.1088/1361-648X/ac553c.

[36] T.L. Dora, A. Owhal, T. Roy, S.U. Belgamwar, S. Goel, H.Y. Nezhad, R.R. Mishra, Thermo-physical characteristics of 3C-SiC structure subjected to microwave exposure: A molecular dynamics study, Mater. Today Commun. 35 (2023) 105693. https://doi.org/10.1016/j.mtcomm.2023.105693.

[37] P. Vashishta, R.K. Kalia, A. Nakano, J.P. Rino, Interaction potential for silicon carbide : A molecular dynamics study of elastic constants and vibrational density of states for crystalline and amorphous silicon carbide Interaction potential for silicon carbide : A molecular dynamics study of elastic c, J. Appl. Phys. Phys. 101 (2007) 1–12. https://doi.org/10.1063/1.2724570.

[38] S. Sun, X. Peng, H. Xiang, C. Huang, B. Yang, F. Gao, T. Fu, Molecular dynamics simulation in single crystal 3C-SiC under nanoindentation: Formation of prismatic loops, Ceram. Int. 43 (2017) 16313–16318. https://doi.org/10.1016/j.ceramint.2017.09.003.

[39] B. Zhu, D. Zhao, H. Zhao, A study of deformation behavior and phase transformation in 4H-SiC during nanoindentation process via molecular dynamics simulation, Ceram. Int. 45 (2019) 5150–5157. https://doi.org/10.1016/j.ceramint.2018.10.261.

[40] L. Zhao, J. Zhang, J. Zhang, A. Hartmaier, Atomistic investigation of machinability of monocrystalline 3C–SiC in elliptical vibration-assisted diamond cutting, Ceram. Int. 47 (2021) 2358–2366. https://doi.org/10.1016/j.ceramint.2020.09.078.

[41] E.M. Nordhagen, H.A. Sveinsson, A. Malthe-Sørenssen, Diffusion-driven frictional aging in silicon carbide, Tribol. Lett. 71 (2023) 1–11. https://doi.org/10.1007/s11249-023-01762-z.

[42] P. Hirel, Atomsk: A tool for manipulating and converting atomic data files, Comput. Phys. Commun. 197 (2015) 212–219. https://doi.org/10.1016/j.cpc.2015.07.012.

[43] K. Vollmayr-Lee, Introduction to molecular dynamics simulations, Am. J. Phys. 88 (2020) 401–422. https://doi.org/10.1119/10.0000654.

[44] A. Stukowski, Visualization and analysis of atomistic simulation data with OVITO-the Open Visualization Tool, Model. Simul. Mater. Sci. Eng. 18 (2010). https://doi.org/10.1088/0965-0393/18/1/015012.

[45] A. Fakhri, S. Rashidi, M. Asif, A.A. Ibrahim, Microwave-assisted synthesis of SiC nanoparticles for the efficient adsorptive removal of nitroimidazole antibiotics from aqueous solution, Appl. Sci. 7 (2017) 1–12. https://doi.org/10.3390/app7020205.

[46] N.M. Sultan, T.M.B. Albarody, H.K.M. Al-Jothery, M.A. Abdullah, H.G. Mohammed, K.O. Obodo, Thermal Expansion of 3C-SiC Obtained from In-Situ X-ray Diffraction at High Temperature and First-Principal Calculations, Materials (Basel). 15 (2022). https://doi.org/10.3390/ma15186229.

[47] P. Zhou, T. Sun, X. Shi, J. Li, Y. Zhu, Z. Wang, Atomic-scale study of vacancy defects in SiC affecting on removal mechanisms during nano-abrasion process, Tribol. Int. 145 (2020) 106136. https://doi.org/10.1016/j.triboint.2019.106136.

[48] M. Tahani, E. Postek, L. Motevalizadeh, T. Sadowski, Effect of Vacancy Defect Content

on the Interdiffusion of Cubic and Hexagonal SiC/Al Interfaces: A Molecular Dynamics Study, Molecules. 28 (2023) 1–17. https://doi.org/10.3390/molecules28020744.

[49] J. Xi, C. Liu, I. Szlufarska, Effects of point defects on oxidation of 3C–SiC, J. Nucl. Mater. 538 (2020) 152308. https://doi.org/10.1016/j.jnucmat.2020.152308.

[50] D. Sheppard, R. Terrell, G. Henkelman, Optimization methods for finding minimum energy paths, J. Chem. Phys. 128 (2008). https://doi.org/10.1063/1.2841941.

[51] M.R. Hestenes, E. Stiefel, Methods of conjugate gradients for solving linear systems, J. Res. Natl. Bur. Stand. (1934). 49 (1952) 409. https://doi.org/10.6028/jres.049.044.

[52] William G. Hoover, Canonical dynamics: Equilibrium phase-space distributions, Phys. Rev. A. 31 (1985) 1695–1697. https://doi.org/10.1007/BF00419952.

[53] D.J. Evans, B.L. Holian, The Nose-Hoover thermostat, J. Chem. Phys. 83 (1985) 4069–4074. https://doi.org/10.1063/1.449071.

[54] N.J. English, C.J. Waldron, Perspectives on external electric fields in molecular simulation: Progress, prospects and challenges, Phys. Chem. Chem. Phys. 17 (2015) 12407–12440. https://doi.org/10.1039/c5cp00629e.

[55] A. V. Rozhkov, S.K. Ignatov, E. V. Suleimanov, Resonant increase of ionic conductance of yttria-stabilized zirconia in an alternating external electric field, J. Solid State Electrochem. 27 (2023) 1177–1184. https://doi.org/10.1007/s10008-023-05420-1.

[56] A. Estejab, R.A. García Cárcamo, R.B. Getman, Influence of an electrified interface on the entropy and energy of solvation of methanol oxidation intermediates on platinum(111) under explicit solvation, Phys. Chem. Chem. Phys. 24 (2022) 4251–

4261. https://doi.org/10.1039/d1cp05358b.

[57] Y. Zhang, L. Wu, X. Guo, Y.G. Jung, J. Zhang, Molecular dynamics simulation of electrical resistivity in sintering process of nanoparticle silver inks, Comput. Mater. Sci. 125 (2016) 105–109. https://doi.org/10.1016/j.commatsci.2016.08.047.

[58] Y. Iwai, H. Higashi, H. Uchida, Y. Arai, Molecular dynamics simulation of diffusion coefficients of naphthalene and 2-naphthol in supercritical carbon dioxide Yoshio, Fluid Phase Equilib. 127 (1997) 251–261.

[59] F. Gao, W.J. Weber, M. Posselt, V. Belko, Atomistic study of intrinsic defect migration in 3C-SiC, Phys. Rev. B - Condens. Matter Mater. Phys. 69 (2004) 2–6. https://doi.org/10.1103/PhysRevB.69.245205.

[60] W. Yan, Q. Xie, T. Gao, X. Guo, Microstructural evolution of SiC during melting process, Mod. Phys. Lett. B. 27 (2013) 6–8. https://doi.org/10.1142/S021798491350231X.

[61] S. Jha, V. Ponce, J.M. Seminario, Investigating the effects of vacancies on self-diffusion in silicon clusters using classical molecular dynamics, J. Mol. Model. 24 (2018). https://doi.org/10.1007/s00894-018-3814-5.

[62] S. Xu, G. Zhong, C. Chen, R. Michael, S.M. Anlage, S. Xu, G. Zhong, C. Chen, M. Zhou, D.J. Kline, R.J. Jacob, H. Xie, S. He, Z. Huang, J. Dai, A.H. Brozena, R. Shahbazian-yassar, Microwave Shock for Nanoparticle Synthesis through Defect Engineering Uniform , Scalable , High-Temperature Microwave Shock for Nanoparticle Synthesis through Defect Engineering, Matter. 1 (2019) 759–769. https://doi.org/10.1016/j.matt.2019.05.022.

[63] I. Dobson, R.F. Cooper, Mechanisms for nonthermal effects on ionic mobility during microwave processing of crystalline solids, J. Mater. Res. 7 (1992) 495–501. https://doi.org/10.1557/JMR.1992.0495.

[64] T. Minh, L. Nguyen, V. Van Hoang, H.T.T. Nguyen, Structural evolution of free-standing 2D silicon carbide upon heating, (2020) 1–7.

[65] K. Sadki, F.Z. Zanane, M. Ouahman, L.B. Drissi, Molecular dynamics study of pristine and defective hexagonal BN, SiC and SiGe monolayers, Mater. Chem. Phys. 242 (2020) 122474. https://doi.org/10.1016/j.matchemphys.2019.122474.

[66] T. Ohshima, A. Uedono, H. Abe, Z.Q. Chen, H. Itoh, M. Yoshikawa, K. Abe, O. Eryu, K. Nakashima, Positron annihilation study of vacancy-type defects in silicon carbide co-implanted with aluminum and carbon ions, Phys. B. 310 (2001) 652–655.

[67] E. Rauls, T. Frauenheim, Theoretical study of vacancy diffusion and vacancy-assisted clustering of antisites in SiC, Phys. Rev. B. 68 (2003) 155208. https://doi.org/10.1103/PhysRevB.68.155208.